Relative Contributions of Inelastic and Elastic Diffuse Phonon Scattering to Thermal Boundary Conductance Across Solid Interfaces

Patrick E. Hopkins[1]

Pamela M. Norris[2]
e-mail: pamela@virginia.edu

Department of Mechanical and Aerospace Engineering,
University of Virginia,
P.O. Box 400746,
Charlottesville, VA 22904-4746

The accuracy of predictions of phonon thermal boundary conductance using traditional models such as the diffuse mismatch model (DMM) varies depending on the types of material comprising the interface. The DMM assumes that phonons, undergoing diffuse scattering events, are elastically scattered, which drives the energy conductance across the interface. It has been shown that at relatively high temperatures (i.e., above the Debye temperature) previously ignored inelastic scattering events can contribute substantially to interfacial transport. In this case, the predictions from the DMM become highly inaccurate. In this paper, the effects of inelastic scattering on thermal boundary conductance at metal/dielectric interfaces are studied. Experimental transient thermoreflectance data showing inelastic trends are reviewed and compared to traditional models. Using the physical assumptions in the traditional models and experimental data, the relative contributions of inelastic and elastic scattering to thermal boundary conductance are inferred. [DOI: 10.1115/1.2995623]

Keywords: thermal boundary conductance, diffuse phonon scattering, elastic scattering, inelastic scattering, nanoscale solid interfaces

Introduction

An understanding of the basic energy transport mechanisms involved in interfacial thermal transport is critical for thermal management of nanostructured devices. When the length scale of a device is comparable to or shorter than the host material's thermal diffusion length, which is often the case for modern nanoscale devices, heat transport away from the active regions is greatly affected by the interfacial properties [1]. An ever increasing challenge in the development of these devices is successfully engineering the heat transport across the interfaces to control the thermal responses experienced in the materials in the devices. This involves a fundamental understanding of the thermal boundary conductance, h_{BD}, at the specific interfaces.

This study examines the relative contributions of inelastic and elastic diffuse phonon scattering on thermal boundary conductance. Several models to predict thermal boundary conductance are discussed in detail and compared to experimental data. Based on the assumptions of these models, a new model to predict the maximum h_{BD} due to inelastic scattering is presented. Using this new model, the relative contributions of elastic and inelastic scattering on h_{BD} are examined.

Models for Phonon Thermal Boundary Conductance

In an attempt to predict thermal boundary conductance at low temperatures, Little [2] proposed the acoustic mismatch model (AMM) to account for the specular scattering of phonons at an interface between two materials. In the following derivation of the AMM and subsequent discussion, side 1 will refer to the side of the interface with the "softer" material and side 2 will refer to the side of the interface with the "stiffer" material. The softer materials are characterized by their lower phonon velocities, smaller phonon vibrational spectrum, and lower Debye temperatures compared to the stiffer materials, which have higher phonon velocities, larger phonon vibrational spectrum, and higher Debye temperatures. For example, consider a metal/dielectric system in which phonons are propagating in a metallic film such as Pb (the lower Debye temperature, softer, material) toward the interface with a dielectric substrate such as diamond (the higher Debye temperature, stiffer, material). In this case, the metallic Pb film is referred to as side 1 and the dielectric diamond substrate as side 2. Table 1 gives phonon velocities, vibrational cutoff frequencies, and Debye temperatures for several materials of interest in this work. The net heat flux occurring from side 1 to side 2 can be calculated by

$$\dot{q} = h_{BD}\Delta T \tag{1}$$

Using the analogy between photons and phonons as wavepackets of energy, the intensity of phonons [3] is used to calculate the heat flux determined from the equation of phonon radiative transfer (EPRT) [4]. The heat flux is expressed as

$$\dot{q} = \frac{1}{2}\sum_j \int_0^{\pi/2} \int_0^{\omega_{1,j}^c} D_{1,j}(\omega) n(\omega,T) \hbar\omega \nu_{1,j} \alpha_{1,j}(\phi,\omega) \times \cos(\phi)\sin(\phi) d\omega d\phi = h_{BD}\Delta T \tag{2}$$

where ω^c is the cutoff frequency, $D(\omega)$ is the density of states, $n(\omega,T)$ is the Bose–Einstein phonon distribution function, ω is the

[1]Present address: Engineering Sciences Center, Sandia National Laboratories, P.O. Box 5800, Albuquerque, NM 87185-0346.

[2]Author to whom correspondence should be addressed.

Contributed by the Heat Transfer Division of ASME for publication in the JOURNAL OF HEAT TRANSFER. Manuscript received February 13, 2008; final manuscript received August 6, 2008; published online January 5, 2009. Review conducted by Jayathi Murthy. Paper presented at the 2007 ASME International Mechanical Engineering Congress (IMECE2007), Seattle, WA, November 10–16, 2007.

Table 1 Debye temperature [8,24,25], longitudinal and transverse phonon velocities [19,25], and calculated cutoff frequencies of materials of interest in this study

Material	θ_D (K)	ν_L (m s^{-1})	ν_T (m s^{-1})	$\omega_L^c \times 10^{-13}$ (s^{-1})	$\omega_T^c \times 10^{-13}$ (s^{-1})
Al_2O_3	1035	10,890	6450	12.1	7.19
AlN	1150	11,120	6267	15.8	8.89
Au	165	3390	1290	5.14	1.96
Bi	119	1543	1107	1.45	1.04
Diamond	2230	17,500	12,800	30.2	22.1
Pb	105	2350	970	2.96	1.22
Pt	240	4174	1750	6.60	2.77

phonon frequency, ν is the phonon velocity, and $\alpha(\phi,\omega)$ is the phonon transmission probability. In this analysis, a local thermodynamic equilibrium is assumed around the phonon scattering event, so local temperatures can be defined. The subscripts "1" and "j" refer to the side and the phonon mode (longitudinal or transverse), respectively. Rearranging Eq. (2) and for the limit of ΔT approaching zero, the AMM is given by

$$h_{BD} = \frac{1}{2}\sum_j \int_0^{\pi/2} \int_0^{\omega_{1,j}^c} D_{1,j}(\omega)\frac{\partial n(\omega,T)}{\partial T}\hbar\omega\nu_{1,j}\alpha_{1,j}(\phi,\omega) \times \cos(\phi)\sin(\phi)d\omega d\phi \tag{3}$$

Note, in the AMM, the transmission probability is a function of incident angle. Although Eq. (3) has been shown to predict h_{BD} relatively well at low temperatures ($T<7$ K) and at ideal interfaces where specular scattering is probable [5], this represents only a very limited population of interfaces in modern devices, which may operate at higher temperatures and have disordered regions near the interface that induce diffuse scattering.

To account for this type of phonon scattering, Swartz and Pohl [6] developed the diffuse mismatch model (DMM) to predict h_{BD} at more realistic interfaces. The DMM theory assumes elastic scattering, that is, upon scattering a phonon forgets where it came from and thus the probability of reflection from one side equals the probability of transmission from the other. The probability that a phonon will scatter into a given side of the interface is thus independent of where it came from, but rather it is proportional to the density of phonon states on that side and is restricted by the principle of detailed balance.

To apply the DMM in its simplest form, the following assumptions must be made [7]: (1) phonons are elastically scattered, i.e., a phonon from side 1 with frequency ω can only emit a phonon from the interface with the same frequency ω; (2) phonon scattering is completely diffuse, i.e., a scattered phonon has no memory of the mode (longitudinal or transverse) or direction of the incident phonon; and (3) the materials on both sides of the interface are elastically isotropic, i.e., the longitudinal and transverse acoustic velocities are constant in all crystallographic directions. Assumption (3) relaxes the angle dependence in Eq. (3), which leads to

$$h_{BD}^{\mathrm{DMM}} = \frac{1}{4}\sum_j \nu_{1,j}\int_0^{\omega_{1,j}^c} \alpha_1(\omega)\hbar\omega D_{1,j}(\omega)\frac{\partial n(\omega,T)}{\partial T}d\omega \tag{4}$$

The linear Debye approximation for the phonon dispersion will be used to calculate the phonon density of states. The cutoff frequency of each phonon mode j on side 1 can be calculated for the separate phonon modes. Assuming Debye dispersion, the cutoff frequency can be calculated by $\omega_{1,j}^c = \nu_{1,j}(6\pi^2 N_1)^{1/3}$, where N_1 is the total number of oscillators per until volume of side 1 [8]. In cubic structures (such as metal with one atom per unit cell), N_1 is simply the atomic density, calculated by $N_1 = \rho N_A / M$, where ρ is the mass density, N_A is Avogadro's number, and M is the atomic weight. However, in structures with more than one atom per unit cell (for example, diamond structures with diatomic basis such as Si or diamond), the number of primitive cells per unit volume must be divided by the number of atoms in the basis [9]. Therefore, for a diatomic basis, $N_1 = \rho N_A/(2M)$.

Due to the assumption of diffuse scattering, the probability of transmission from side 1 to side 2 is the same as the probability of reflection from side 2 to side 1, i.e., $\alpha_1(\omega) = 1 - \alpha_2(\omega)$. Therefore, according to the principle of detailed balance, the phonon transmission probability is calculated by [6]

$$\alpha_1(\omega) = \frac{\sum_j \nu_{2,j}^{-2}}{\sum_j \nu_{2,j}^{-2} + \sum_j \nu_{1,j}^{-2}} = \alpha_1 \tag{5}$$

This simplified transmission coefficient is a result of assuming a Debye density of states and elastic scattering. The transmission probability calculated with the Debye density of states agrees well with the transmission of two simple structures calculated with a more realistic density of states and molecular dynamics simulations (MDSs) [10,11]. The DMM has been shown to predict the response of higher temperature interfaces ($T>15$ K) relatively well [5,6]. However, at much higher temperatures, the DMM has been shown to do a poor job of predicting the value of h_{BD}, in some cases underpredicting [12] while in other cases overpredicting [7,12–14].

Another model for h_{BD}, the phonon radiation limit (PRL), estimates the maximum conductance for interfacial transport due to elastic scattering [15]. The development of the PRL is very similar to that of the DMM. However, the PRL assumes that all of the phonons in side 2 up below the cutoff frequency in side 1 (assuming $\omega_1^c < \omega_2^c$) contribute to thermal transport though elastic collisions ($\alpha=1$). With these assumptions, the PRL is given as

$$h_{BD}^{\mathrm{PRL}} = \frac{1}{4}\sum_j \nu_{2,j}\int_0^{\omega_{1,j}^c} \hbar\omega D_{2,j}(\omega)\frac{\partial n(\omega,T)}{\partial T}d\omega \tag{6}$$

which represents the maximum conductance due to elastic scattering.

The applicability of all of the aforementioned models is limited to interfaces in which thermal transport is dominated by elastic phonon scattering. Inelastic phonon scattering has been shown to offer an additional channel for thermal transport, which can lead to different values and trends than predicted with available models [10,16,17]. In the classical limit (for real materials $T>\theta_{D,1}$, the Debye temperature of side 1, the lower Debye temperature material), h_{BD} calculated by either the DMM or PRL is relatively independent of temperature. The only temperature dependent part of either model is in the distribution function, which at temperatures well above the Debye temperature becomes constant. Because these models do not assume any inelastic scattering, the models are independent of temperature at high temperatures (when $T>\theta_{D,1}$). To check the temperature dependence of h_{BD}, Stevens et al. [10] conducted several molecular dynamic simulations at a range of temperatures. A strong linear relationship was observed in the results of the MD calculations. This linear trend in h_{BD} when $T>\theta_{D,1}$ has been observed experimentally with transient

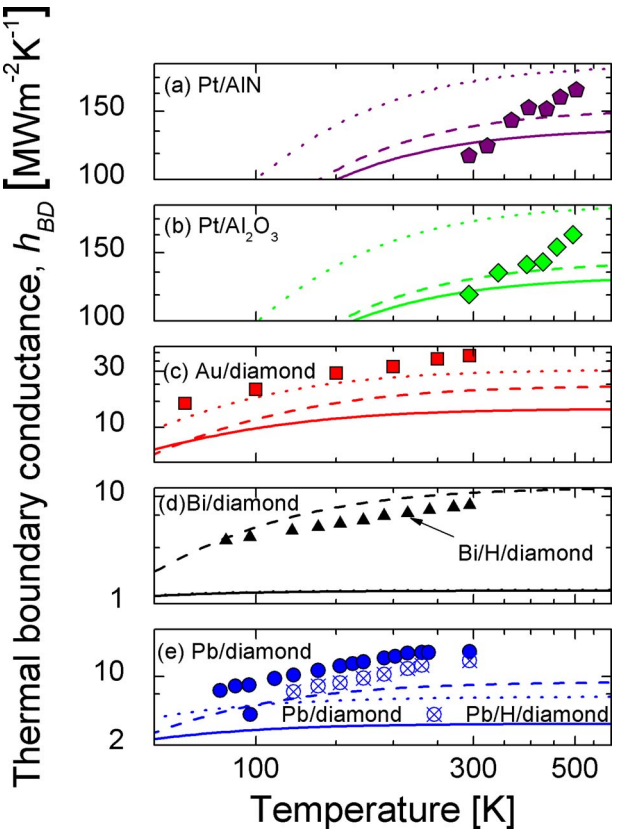

Fig. 1 DMM (solid line), PRL (dotted line), and JFDMM (dashed line) calculations compared to temperature dependent TTR data on (*a*) Pt/AlN [17], (*b*) Pt/Al_2O_3 [17], (*c*) Au/diamond [14], (*d*) Bi/H/diamond [16], and (*e*) Pb/diamond and Pb/H/diamond [16]. Note the similar temperature dependent trends of the DMM and PRL due to their assumption of elastic scattering.

thermoreflectance (TTR) pump-probe measurements. Stoner and Maris [14] have shown this linear trend for a Au film on a diamond substrate. This trend was shown on several other film substrate material systems at low temperatures by Lyeo and Cahill [16] and at high temperatures by Hopkins et al. [17]. In all cases, values and trends in the experimental data differ from those predicted by the DMM and PRL.

An underlying assumption governing the DMM and PRL is that a phonon transmits energy across an interface by emitting a phonon with the same frequency, i.e., the phonons are elastically scattered. Therefore, as the interface temperature is driven up above the Debye temperature of the softer material, h_{BD} is predicted to be relatively constant by the DMM. For example, Pb/diamond in Fig. 1 where $\theta_{D\_Pb}=105$ K and $\theta_{D\_diamond}=2200$ K [8]. This is a result of the change in phonon population with temperature predicted by the Bose–Einstein distribution function. At temperatures close to a material's Debye temperature, the change in phonon population with temperature becomes linear. The DMM is a function of the temperature derivative of the Bose–Einstein distribution, which results in the constant h_{BD} predicted at higher temperatures ($T > \theta_{D\_Pb}$). Assuming elastic scattering, the h_{BD} predictions would follow a trend relating to the change in the Pb phonon population with temperature. However, if inelastic phonon processes occur (i.e., a phonon with frequency $\omega^c_{diamond}$ scatters into several phonons with frequencies below ω^c_{Pb}), then the change in h_{BD} with temperature would be related to the change in the diamond phonon population in addition to the Pb population.

Using this approach, Hopkins and Norris [18] developed a simple correction to the DMM to account for the discrepancy between the DMM and the experimental data in the event of inelastic scattering. By blending the vibrational spectra of the film and substrate materials, an approximation was developed for the contribution of these inelastic modes with a diffuse scattering assumption, the joint frequency diffuse mismatch model (JFDMM). The JFDMM assumes the same form as the DMM (Eq. (4)) but uses a modified phonon velocity that is taken as a weighted average of the velocities of the phonons of sides 1 and 2. Consequently, this results in a weighted average of the phonon spectra used in the h_{BD} calculation, given by

$$D_{\mathrm{mod},j} = \frac{\omega^2}{2\pi^2 \nu_{\mathrm{mod},j}^{\ 3}}, \quad \omega \leqslant \omega^c_{\mathrm{mod},j} \tag{7}$$

$$\omega^c_{\mathrm{mod},j} = \nu_{\mathrm{mod},j}\{6\pi^2(\xi_1 N_1 + \xi_2 N_2)\}^{1/3} \tag{8}$$

$$\nu_{\mathrm{mod},j} = \xi_1 \nu_1 + \xi_2 \nu_2 \tag{9}$$

where the weighting factor ξ is simply a percentage of the composition of each material in the unit volume, mathematically expressed as

$$\xi_1 = \frac{\frac{N_1}{N_2} M_1}{\frac{N_1}{N_2} M_1 + M_1} \tag{10}$$

where M is the atomic mass. This approximation introduces high frequency phonons that are available in the vibrational spectrum in side 2 but not side 1 into the incident heat flux. The JFDMM increases the prediction of h_{BD} by a factor that is proportional to the side 2 vibrational spectrum, giving an approximation for inelastic scattering. The transmission coefficient for the JFDMM is still assumed to be calculated with Eq. (5); note that this relaxes the assumption of detailed balance since the JFDMM assumes a modified phonon flux.

Figure 1 compares the predictions from the DMM, PRL, and JFDMM to experimental TTR data taken on several different material systems over a wide range of temperatures. This figure compares predictive trends to data on (a) Pt/AlN (Hopkins et al.) [17], (b) Pt/Al_2O_3 (Hopkins et al.) [17], (c) Au/diamond (Stoner and Maris) [14], (d) Bi/H/diamond (Lyeo and Cahill) [16], and (e) Pb/diamond and Pb/H/diamond (Lyeo and Cahill) [16]. The model calculations use elastic constants to calculate phonon velocities and material properties to calculate the cutoff frequencies [19]. Note that the models cannot distinguish between different deposition or interface conditions [20], so the predictions by the models on the hydrogen terminated and non-hydrogen-terminated substrates are the same. In Fig. 1, the DMM is represented by the solid line, the PRL is represented by the dotted line, and the JFDMM is represented by the dashed line. Note that the JFDMM predicts a closer value and better temperature dependent trend to the experimental data than the DMM, and in most cases the PRL. Since the DMM and PRL both assume elastic scattering of frequencies only up to the side 1 cutoff frequency, these models share the same trend with temperature. The JFDMM, however, shows a different temperature dependent trend that is more in line with the experimental data since it assumes phonons with frequencies higher than the cutoff frequency in side 1 can participate in h_{BD}. These data represent material systems that show some evidence of inelastic scattering at these temperatures.

Inelastic Phonon Radiation Limit

Although the JFDMM shows improvement in h_{BD} predictions in the event that inelastic phonon scattering dominates interfacial transport, this method makes necessary assumptions about phonon transport that deserve further attention. The main assumption of the JFDMM is that a fraction of the available phonon states in the substrate are present in the film. In actuality, the atoms around the interface are vibrating at joint modes by Newton's law of motion [21]. The maximum allowable frequency for these joint modes is

the substrate cutoff frequency. However, dampening of these modes will occur due to the differing interatomic forces of the film and substrate. This prevents the joint modes from oscillating at certain frequencies. This continuum phenomenon is paralleled quantum mechanically in the JFDMM through the weighted average of two materials' phonon states in the incident flux. The weighing factor, ξ, reflects the dampening of the substrate modes, and is used to enhance the incident phonon flux to take into account the joint vibrations that are allowed after dampening effects. However, without computationally expensive computer simulations or a rigorous theoretical treatment, this weighting factor cannot be explicitly determined for every phonon mode, and therefore should be viewed as an estimation of the joint modes participating in h_{BD}. That being said, the JFDMM can be viewed as a starting point for estimating the maximum h_{BD} due to inelastic scattering.

Consider atoms vibrating at joint modes around the interface with no dampening effects. Therefore, these atoms can vibrate at all allowable frequencies up to the maximum allowed frequency in the substrate. Atoms on side 1 and side 2 will be coupled in joint vibrational modes with frequencies up to the cutoff frequency on side 2. This is paralleled in the quantum treatment by forcing $\xi_1=0$ and $\xi_2=1$, which conceptually is treating h_{BD} as a function of the incident phonon flux from side 2 transmitted into side 1. This simplifies Eqs. (7)–(9) to $D_{\mathrm{mod},j}=D_{2,j}$, $\omega^c_{\mathrm{mod},j}=\omega^c_{2,j}$, and $\nu_{\mathrm{mod},j}=\nu_{2,j}$, respectively, and redefines Eq. (4) in terms of the flux transmitted from side 2 to side 1, given as

$$h_{BD}^{\mathrm{inel}}=\frac{1}{4}\sum_j \nu_{2,j}\int_0^{\omega^c_{2,j}} \alpha_2^{\mathrm{inel}}(T)\hbar\omega D_{2,j}(\omega)\frac{\partial n(\omega,T)}{\partial T}d\omega \qquad (11)$$

From the nature of diffuse scattering, the inelastic transmission probability is $\alpha_2^{\mathrm{inel}}(T)=1-\alpha_1^{\mathrm{inel}}(T)$, which is different from the elastic transmission probability calculated with Eq. (5). Equation (11) allows for the possibility of higher frequency phonons that do not exist in the film to participate in h_{BD}. Without knowledge of the explicit temperature dependence of α_2, h_{BD} cannot be calculated. However, examining Eq. (11) along with experimental data can give important understanding of the role of inelastic phonon scattering in thermal boundary conductance.

Consider the case where all available substrate phonons are participating in h_{BD}. In this case, the probability that a phonon on side 2 is inelastically transmitted (i.e., breaks down into lower frequency phonons and transmitted into side 1) is 1. By letting $\alpha_2=1$, Eq. (11) becomes an expression for the largest allowable thermal boundary conductance due to inelastic scattering, or an inelastic phonon radiation limit (IPRL), expressed as

$$h_{BD}^{\mathrm{IPRL}}=\frac{1}{4}\sum_j \nu_{2,j}\int_0^{\omega^c_{2,j}} \hbar\omega D_{2,j}(\omega)\frac{\partial n(\omega,T)}{\partial T}d\omega \qquad (12)$$

The IPRL assumes that all side 2 phonons are transmitted into side 1, and does not explicitly take into account elastic or inelastic scattering processes. However, by allowing all frequencies of phonons in side 2 to transmit energy into side 1, which has the lower cutoff frequency, inelastic scattering is implied. Note that in this limit, similar to the JFDMM, which also takes into account some inelastic scattering, the assumption of equilibrium is relaxed and therefore the principle of detailed balance is not enforced. Also, in the case of an interface in a homogeneous material (i.e., an "imaginary" interface between two of the same materials), the IPRL does not impose any unphysical interface resistance and gives the same thermal flux across an imaginary interface in a homogeneous material as that predicted by the Fourier law. The other models discussed thus far require accurate knowledge of interface transmission probability and the use of a diffusion-transmission interface correction [22] to relax to flux predicted by the Fourier law ensuring thermal flux continuity.

Equation (12) is solely dependent on the acoustic properties of side 2, so in the IPRL, h_{BD} on any film/substrate system only depends on the stiffer material. This is apparent in Figs. 2 and 3, which compare the temperature dependent h_{BD} data from Fig. 1 to their respective IPRL and PRL calculations. The experimental data are graphed on the same plot as their PRL calculations. The IPRL calculations are shown in the lower plots of the figures since the values of the IPRL are orders of magnitude greater than the data and the PRL. However, the separate plots allow for easy comparisons of temperature trends between the models and the data.

The IPRL calculations for the three material systems in Fig. 2 are all identical, since the IPRL is only dependent on the higher

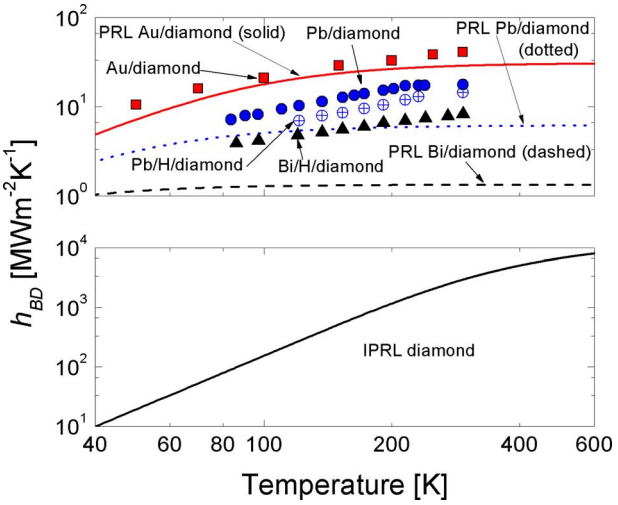

Fig. 2 (Top) Experimental measurements of h_{BD} for various interfaces (see Fig. 1) compared to their corresponding PRL. The PRL predicts a constant h_{BD} at temperatures above the Debye temperature of the lower Debye temperature material. (Bottom) Inelastic phonon radiation limit for the four material systems in the top graph. The IPRL shows a linear increase over a temperature range of 100–400 K, the same trend that is shown in the experimental data. Note, however, that the slope of the linear increase in the IPRL is much greater than the slope of the linear increase in the data.

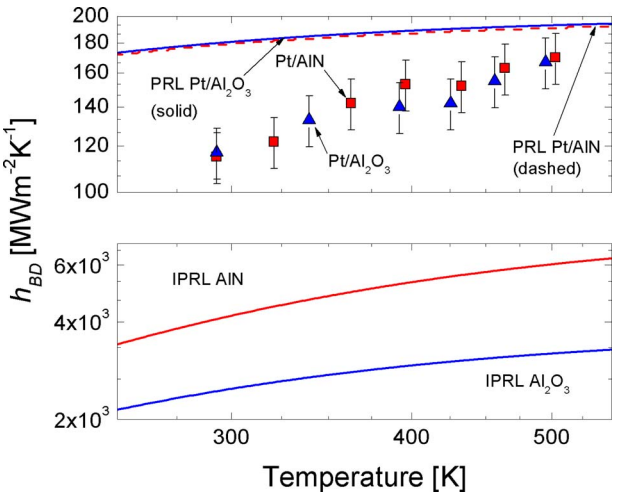

Fig. 3 (Top) Experimental measurements of h_{BD} for Pt/Al_2O_3 and Pt/AlN (see Fig. 1) compared to their corresponding PRL. (Bottom) Inelastic phonon radiation limit for the two material systems in the top graph. The increase in h_{BD} over the temperature range of interest is greater in the IPRL than in the slope of the linear increase in the data, which is greater than the increase in the PRL.

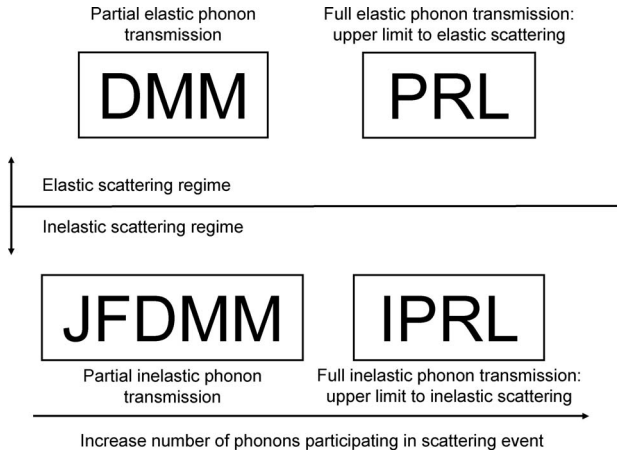

Fig. 4 Regime map of thermal boundary conductance models that takes into account various degrees of elastic and inelastic diffuse phonon scattering. The DMM and PRL, which take into account varying degrees of elastic scattering, are paralleled with the JFDMM and IPRL, which take into account varying degrees of inelastic scattering.

Debye temperature material (side 2). The PRL, on the other hand, depends on the cutoff frequency of the lower Debye temperature material (side 1), so therefore is specific for each film/substrate material system. In all cases, the IPRL is greater than the PRL, which is intuitive since the PRL assumes that only a certain fraction (up to the film cutoff frequency) of substrate phonons are participating in h_{BD} where the IPRL assumes that all available substrate phonons can participate in h_{BD}. In addition, notice that the PRL predicts h_{BD} as a constant value above the film's Debye temperature (similar to the DMM), where the IPRL predicts a linear change of h_{BD} with temperature, similar to the trends in the experimental data. In all cases, the linear change in the IPRL is much greater than the linear change in the data. Figure 3 shows the same calculations as Fig. 2 for the Pt/Al_2O_3 and Pt/AlN data. Note that the IRPL calculations for AlN and Al_2O_3 are vastly different (bottom), yet the experimental data and PRL calculations for the two samples are nearly identical (top). The measured Debye temperatures for AlN and Al_2O_3 are nearly identical, which would mean they have similar maximum cutoff frequencies. However, with a Debye approximation, the calculations of the cutoff frequencies do not match. This could be a result of assuming that these solids can be treated as Debye solids, which may not be completely accurate for complex dielectrics such as AlN or Al_2O_3. However, for the purpose of this analysis, the Debye solid is assumed for all materials since it allows for a simple calculation to elucidate important physics in interfacial phonon scattering processes.

Figure 4 shows a regime map of the four different models for thermal boundary conductance driven by diffuse phonon scattering. The DMM, which takes into account partial phonon transmissivity, is the elastic version of the JFDMM, which takes into account partial phonon transmissivity during inelastic scattering. The upper limits to the DMM and JFDMM models are the PRL and the IPRL, respectively, which assume a phonon transmissivity of unity during elastic and inelastic interfacial phonon scattering, respectively.

Relative Contributions of Inelastic and Elastic Phonon Scattering

From the trends in the IPRL as compared to the PRL and experimental data, the relative contributions of elastic and inelastic scattering can be examined. Above the film's Debye temperature, it is apparent that contributions from elastic scattering will result in a constant h_{BD}. However, inelastic scattering events will drive the linear trend in h_{BD}. Therefore, the total thermal boundary conductance in the classical limit ($T > \theta_D$) will be a blend of both the constant elastic and temperature dependent inelastic phonon scattering contributions, which can be mathematically expressed as

$$h_{BD}(T) = h_{BD}^{\text{el}} + h_{BD}^{\text{inel}}(T) \tag{13}$$

where the superscripts el and inel denote the elastic and inelastic contributions to h_{BD}. This is similar to the phenomenological observation by Stevens et al. [10] based on MD simulations. Equation (13) separates the elastic and inelastic contributions to h_{BD} by assuming that these two energy transfer mechanisms can be treated as two thermal pathways in parallel. Assuming that the elastic and inelastic scattering contributions to h_{BD} can be separated is valid since in acoustically mismatched materials such as those of interest in this work, the number of phonons at any available frequency, ω, in side 1 is much greater than the number of phonons at that same frequency ω in side 2, so phonons of frequencies ω in the side 1 vibrational spectrum can participate in both elastic and inelastic scattering events.

Since the PRL and the IPRL represent the upper limit to elastic and inelastic scattering, it is expected that the elastic and inelastic contributions to h_{BD} will be some fraction of the PRL and IPRL, respectively. Therefore, Eq. (13) can be written more explicitly as

$$h_{BD}(T) = Ah_{BD}^{\text{PRL}} + B(T)h_{BD}^{\text{IPRL}}(T) \tag{14}$$

Where h_{BD}^{PRL} is the PRL and $h_{BD}^{\text{IPRL}}(T)$ is calculated by Eq. (12). The coefficients A and $B(T)$ are coefficients representing the fraction of the maximum possible conductance due to each scattering process and will be determined from the experimental data in the next section. Although A can be estimated using Eq. (5) so that $A = 1 - \alpha_1 = \alpha_2$ and $h_{BD}^{\text{el}} = Ah_{BD}^{\text{PRL}} = [1 - \alpha_1]h_{BD}^{\text{PRL}}$ since only elastic scattering is dealt with in this case, the fundamental assumptions driving the evaluation of α are flawed, even in the elastic limit [23]. For example, in calculating Eq. (5), equilibrium is assumed (principle of detailed balance) although thermal transport is inherently a nonequilibrium process. Also, in the limit that both materials adjacent to the interface are the same, Eq. (5) becomes 50%. However, in this case, since there is no difference in the acoustic properties, phonon transmission should be 100%.

The temperature dependency of the inelastic phonon transmission coefficient, $B(T)$, arises from the fact that as temperature increases, there are proportionately more substrate phonons available to break down and scatter with lower frequency side 1 phonons. This temperature dependency is apparent from the differing linear slopes of the experimental data and the IPRL over the temperature range of interest. Therefore, Eq. (11) can be rewritten as

$$h_{BD}^{\text{inel}} = \frac{1}{4}\sum_j \nu_{2,j} \int_0^{\omega_{2,j}^c} \alpha_2^{\text{inel}}(T)\hbar\omega D_{2,j}(\omega)\frac{\partial n(\omega,T)}{\partial T}d\omega = B(T)h_{BD}^{\text{IPRL}} \tag{15}$$

where $\alpha_2^{\text{inel}}(T) = B(T)$. It is apparent in the data in Figs. 2 and 3 that the temperature dependency will be some function of the temperature dependencies of the phonon populations of both side 1 and side 2. The JFDMM takes this into account by considering a weighted average of the phonon populations of the two sides. However, this correction results in a temperature independent constant that enhances α_1, and a temperature dependent transmission coefficient should be considered to understand the relative effects of inelastic scattering. Through the principle of detailed balance invoked on the incoming phonon fluxes from sides 1 and 2, Dames and Chen [9] developed a temperature dependent transmission coefficient based on the changes of the phonon population of the two sides, given by

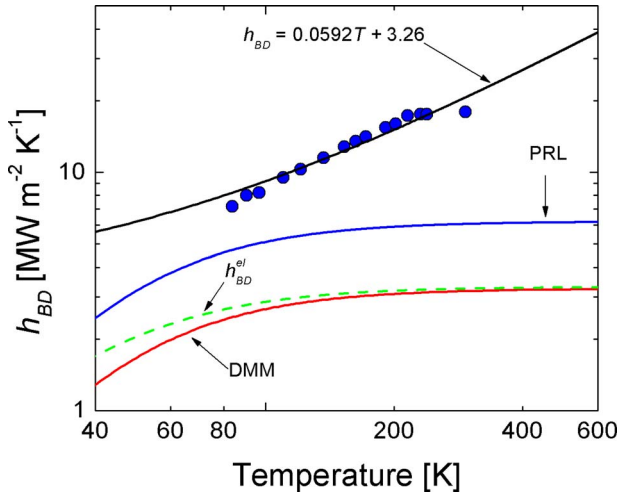

Fig. 5 Measured h_{BD} on Pb/diamond with best fit line extrapolated to determine the *y*-intercept at 3.26 MW m^{-2} K^{-1}, which is assumed as the elastic contribution to h_{BD} in the classical limit. This value is less than the prediction of the PRL, as expected, but agrees well with the predictions from the DMM, validating the transmission coefficient calculations in the DMM for a Pb/diamond interface.

$$\alpha_1^{\text{inel}}(T) = \frac{\sum_j \nu_{2,j} U_{2,j}(T)}{\sum_j \nu_{1,j} U_{1,j}(T) + \sum_j \nu_{2,j} U_{2,j}(T)} \tag{16}$$

where U is the internal energy of the phonon system. Although Eq. (16) gives the correct temperature dependent trend assuming that all phonon frequencies in each material available at any given temperature participate equally to energy transmission, it does not differentiate between inelastic and elastic contributions nor does it take into account the relative contributions from each phonon frequency (i.e., it assumes that all phonon frequencies have an equal probability of participating in phonon scattering events). However, there is some intrinsic frequency dependence on the transmission coefficient, which is contained in the temperature dependence of the experimental data and not contained in the assumptions of Eq. (16).

In order to determine the relative contributions from elastic and inelastic scattering, the coefficients A and $B(T)$ must be examined in greater detail, which can be accomplished by examining h_{BD} data clearly dominated by inelastic scattering. In this analysis, only temperatures in the classical limit of the metal films will be considered (i.e., temperatures above the softer material's Debye temperature). In this limit the data show the linear trend associated with inelastic scattering; however, a fraction of this h_{BD} is expected to be associated with elastic scattering, which is expected to be constant.

To determine h_{BD}^{el}, the linear fit to the data was extended to the *y*-axis to find the *y*-intercept, which is taken as the contribution of elastic scattering in the classical limit. The linear fit of the Pb/diamond data compared to h_{BD}^{PRL}, h_{BD}^{el}, and h_{BD}^{DMM} is shown in Fig. 5. The *y*-intercept is h_{BD}^{el}=3.26 MW m^{-2} K^{-1} where h_{BD}^{PRL} =6.17 MW m^{-2} K^{-1}. As expected, h_{BD}^{PRL} is greater than h_{BD}^{el} determined from experimental data, since not all substrate phonons will be participating in conductance. Comparing these two values yields A=0.53. In this limit, h_{BD}^{DMM}=3.32 MW m^{-2} K^{-1}, which is in excellent agreement with h_{BD}^{el}, indicating that the DMM predicts the elastic contributions to h_{BD} at the heavily mismatched Pb/diamond interface well. Table 2 compares values of h_{BD}^{el} (determined from the *y*-intercept), h_{BD}^{DMM}, h_{BD}^{PRL}, and the coefficient A for six samples in the classical limit. Also listed in Table 2 is the ratio of Debye temperatures of the materials comprising side 1 and side 2 for each interface. This ratio quantifies the degree of acoustic mismatch of each interface—the smaller the ratio, the greater the mismatch between phonon spectra. Note that the agreement between h_{BD}^{el} and h_{BD}^{DMM} is much better for the heavily mismatched samples than for the better matched Pt samples. This is expected since the transmission coefficient calculations become less accurate as the materials become more similar [23]. This indicates that the DMM is a good model for predicting the elastic scattering contribution to thermal boundary conductance, and the transmission coefficient calculated with Eq. (5) becomes more accurate as the adjacent phonon spectra become more dissimilar.

Now that the elastic portion of thermal boundary conductance has been determined, the inelastic contribution can be estimated from the slope of the experimental data. Rearranging Eq. (14), the coefficient representing the transmission of substrate phonons through inelastic scattering can be expressed as

$$B(T) = \frac{h_{BD}(T) - A h_{BD}^{\text{PRL}}}{h_{BD}^{\text{IPRL}}} \tag{17}$$

where $h_{BD}(T)$ is the thermal boundary conductance as a function of temperature determined from the linear fit to the experimental data, and A was determined above. Note that from the discussion of Eq. (15), $B(T)=\alpha_2^{\text{inel}}(T)$. The coefficient $B(T)$ as a function of temperature can be calculated only over the temperature range of the experimental data. However, higher temperature values were determined through a nonlinear regression extrapolation to determine $B(T)$ at all temperatures $T>\theta_D$. Due to the nature of this high temperature extrapolation, above a given temperature the slope of the IPRL decreases to a value that is less than the slope of $h_{BD}(T)$, which causes an unphysical slight linear increase in $B(T)$ resulting in a local minimum. To correct for this unphysical increase in Eq. (17), at temperatures above the local minimum temperature, $B(T)$ is fixed to a constant value of the local minimum. This gives a much more physical trend to $B(T)$ and avoids any error due to the nonlinear extrapolation routine. Figure 6 compares the temperature dependent transmission coefficient that

Table 2 High temperature limits of thermal boundary conductance and the elastic contribution to h_{BD}, the DMM, the PRL, and the predicted h_{BD} based on experimental trends [$h_{BD}(T)$] for six different interfaces. All units are in MW m^{-2} K^{-1}, except A, B, and $\theta_{D,1}/\theta_{D,2}$, which are unitless ratios.

Interface	$\theta_{D,1}/\theta_{D,2}$	h_{BD}^{el}	h_{BD}^{DMM}	h_{BD}^{PRL}	A	B	$h_{BD}(T=\infty)$
Pb/diamond	0.047	3.26	3.31	6.23	0.523	0.00436	58.7
Pb/H/diamond	0.047	1.92	3.31	6.23	0.310	0.00329	41.9
Bi/H/diamond	0.053	2.25	1.32	1.34	1.67	0.00158	22.3
Au/diamond	0.074	16.6	14.4	31.2	0.532	0.00626	96.1
Pt/Al_2O_3	0.21	51.8	130	190	0.261	0.0170	210
Pt/AlN	0.23	51.8	130	190	0.261	0.0280	200

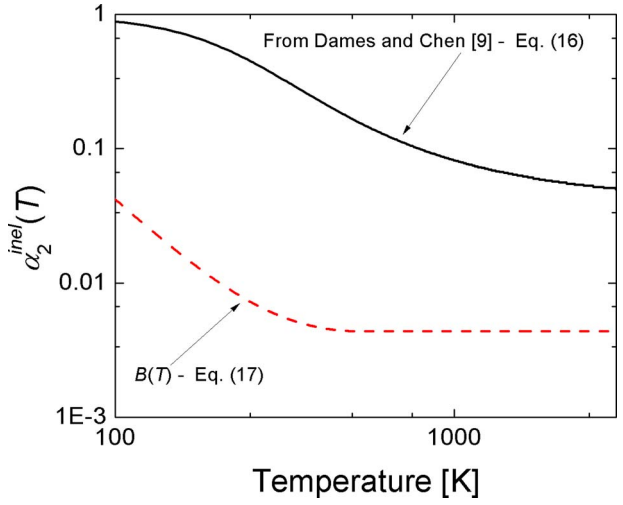

Fig. 6 Comparison of $\alpha_2^{inel}(T)$ determined by $1-\alpha_1^{inel}(T)$ where $\alpha_1^{inel}(T)$ is given by the model derived by Dames and Chen [9] and presented in Eq. (16); and $B(T)$, which is derived in this work and presented in Eq. (17). $B(T)$ decreases to a much lower constant value much more quickly than $\alpha_2^{inel}(T)$ calculated with Eq. (16). The assumption in Eq. (16) is that all phonons of all frequencies have equal probability in transmission, where Eq. (17) is based on experimental data and the IPRL. The smaller phonon transmission of side 2 phonons at higher temperatures could be due to the probability of side 2 phonons breaking down into lower frequency side 1 phonons decreasing as the side 2 phonon frequency increases.

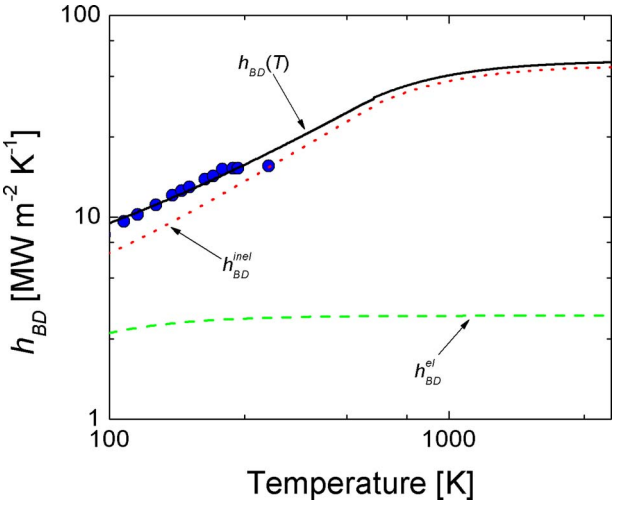

Fig. 7 Inelastic and elastic scattering contributions to h_{BD} of Pb/diamond in the classical limit. The total thermal boundary conductance, $h_{BD}(T)$, shows excellent agreement to the data at low temperatures in the classical limit, and approaches a constant value at higher temperatures that are above the Debye temperature of diamond (or at temperatures that are greater than the Debye temperature of both materials).

takes into account inelastic scattering for side 2 derived by Dames and Chen [9], $\alpha_2^{inel}(T)=1-\alpha_1^{inel}(T)$, where $\alpha_1^{inel}(T)$ is calculated with Eq. (16), to the inelastic transmission coefficient determined from Eq. (17), $B(T)$, for a Pb/diamond interface. $B(T)$ decreases to a much lower constant value much more quickly than $\alpha_2^{inel}(T)$ calculated with Eq. (16). As previously mentioned, Eq. (16) assumes that all phonon frequencies participate equally in transmission and h_{BD}. $B(T)$, however, takes into account the temperature dependent phonon scattering trends in inelastic processes by utilizing the trends encapsulated in the experimental data. The values and trends in $B(T)$ show that as temperature increases and more high frequency phonons become available in side 2 that are not available in side 1 (i.e., the phonon frequencies in side 2 that are above the side 1 cutoff frequency), the transmission of energy from side 2 to side 1 is much less than if assuming all phonon frequencies participate equally in energy transmission as assumed in Eq. (16). This suggests that phonons in side 2 with frequencies much higher than the side 1 cutoff are less likely to participate in inelastic processes than phonons with frequencies that are only slightly higher than the side 1 cutoff. A similar trend was inferred by Hopkins et al. [17], and was attributed to the probability a three-phonon process occurring, which could occur for coupling between a lower frequency side 2 phonon and two side 1 phonons, being higher than the probability of n-phonon processes occurring (where $n>3$), which would have to occur for a higher frequency side 2 phonon to couple with $n-1$ side 1 phonons.

With this, the contributions of elastic and inelastic scattering to h_{BD} were calculated based on experimental data and extended to high temperatures to determine h_{BD} in the classical limit that takes into account inelastic scattering. The inelastic and elastic contributions to h_{BD} for Pb/diamond are shown in Fig. 7, along with $h_{BD}(T)$ calculated from Eq. (14). The high temperature trends follow what is expected when temperatures are driven higher than both materials' Debye temperatures. This same agreement between Eq. (14) and the experimental data and high temperature trends are shown between Eq. (14) and the Bi/diamond, Au/diamond, Pt/Al_2O_3, and Pt/AlN data.

To demonstrate the relative magnitude of inelastic scattering on h_{BD}, the ratio $h_{BD}^{inel}/h_{BD}^{el}$ is plotted versus temperature in the classical regime in Fig. 8 for the six interfaces studied. As expected, the inelastic contribution compared to the elastic contribution to h_{BD} in Pb, Bi, and Au on diamond are more temperature dependent than the relative contribution in the Pt/Al_2O_3 and Pt/AlN samples due to the higher Debye temperature of diamond than Al_2O_3 and AlN. Also, the contribution of inelastic scattering to overall h_{BD} is greater than that of elastic scattering, and the relative contribution of inelastic scattering increases with interface

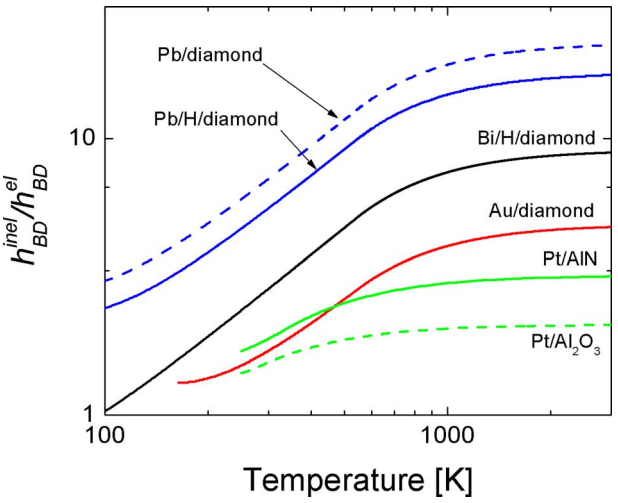

Fig. 8 Relative magnitude of inelastic scattering on h_{BD}. This ratio compares the inelastic contribution to h_{BD} to the elastic contribution as predicted via Eq. (14). The role of inelastic phonon scattering increases as the acoustic mismatch of the film and substrate becomes greater. The range in which h_{BD} should increase linearly with temperature due to inelastic scattering also increases with acoustic mismatch.

acoustic mismatch (i.e., as the film/substrate Debye temperature ratio become smaller). This also leads to the inelastic contribution becoming independent of temperature at higher temperatures in the diamond samples than in the Pt on Al_2O_3 and AlN samples. In fact, the high temperature limit of the Pb, Bi, and Au on diamond samples is not reached until the interface temperature is driven above the melting temperature of the metal, meaning that in nanostructures with Pb, Bi, and Au films adjacent to diamond structures, h_{BD} will continually increase with temperature until melting. Also, in the high temperature limit, as the mismatch between the materials adjacent to the interface grows, the contribution of inelastic phonon scattering to thermal boundary conductance increases.

Conclusions

The accuracy of h_{BD} predictions made using DMM and PRL varies depending on the types of materials comprising the interface. Due to inelastic scattering these models may not be valid at temperatures characteristic of many modern nanodevices and structures since these models do not take into account inelastic phonon scattering. Although the JFDMM provides a simple approximation of the effects of joint vibrational modes on h_{BD} using a Debye approximation, it does not specially examine the contributions due to elastic and inelastic scattering. These contributions can be extracted from the trends and values in the experimental data. To estimate the role of elastic scattering in the classical limit, the y-intercept of the linear trend in the experimental data of h_{BD} as a function of temperature is compared to the PRL in the classical limit. The resulting contribution of elastic scattering in this limit agrees well with the value of h_{BD} predicted by the DMM. This agreement increases with sample mismatch, which validates the DMM as a model to predict the contribution of elastic scattering in heavily mismatched samples. To estimate the role of inelastic scattering in the classical limit, the slope of the experimental data of h_{BD} as a function of temperature is compared to a new model, the IPRL. The IPRL predicts the maximum thermal boundary conductance assuming all substrate phonons of all frequencies are transmitted into the film. The IPRL predictions are compared to the experimental data to effectively determine what percentage of substrate phonons are participating in inelastic scattering beyond those participating in elastic scattering. The role of inelastic scattering to overall h_{BD} is shown to outweigh the role of elastic scattering at the interfaces of interest, with an increasing role of inelastic scattering with interfacial acoustic mismatch. The predictions of inelastic scattering show a linear trend at lower temperatures in the classical limit and predict a constant h_{BD} at higher temperatures, giving an upper limit to thermal boundary conductance that takes into account both elastic and inelastic scattering.

Acknowledgment

The authors would like to thank Rich Salaway, Jennifer Simmons, John Duda, Justin Smoyer, and Tom Randolph of the Microscale Heat Transfer Laboratory at U.Va. and Thomas Beechem and Samuel Graham of GA Tech for insightful discussions; Robert Stevens at RIT for insight into molecular dynamics simulations and vibrational energy transport; and Jongsoo Yoon of the Physics Department at U.Va. for critical reading of the manuscript. P.E.H. would like to thank the NSF graduate research fellowship program for funding. The authors gratefully acknowledge financial support from the Office of Naval Research MURI program, Grant No. N00014-07-1-0723.

Nomenclature

A = coefficient relating to elastic scattering in Eq. (14)
B = coefficient relating to inelastic scattering in Eq. (14)
D = phonon density of states per unit volume, s m^{-3}
$\hbar$ = Planck's constant divided by 2π, J s
h_{BD} = thermal boundary conductance, W m^{-2} K^{-1}
M = molecular weight, g mol^{-1}
N = phonon number density, m^{-3}
N_A = Avogadro's number, mol^{-1}
n = Bose–Einstein distribution function
$\dot{q}$ = heat flux, W m^{-2}
T = temperature, K
U = internal energy, J m^{-3}
ν = phonon group velocity, m s^{-1}

Greek Symbols

α = interfacial transmission probability
ϕ = incident angle
ω = angular frequency, s^{-1}
ξ = weighting factor in JFDMM

Subscripts

1 = film, or lower Debye temperature material, or softer material
2 = substrate, or higher Debye temperature material, or stiffer material
j = phonon mode (polarization)
L = longitudinal
mod = modified
T = transverse

Superscripts

c = cutoff
DMM = calculated with the diffuse mismatch model
el = elastic
inel = inelastic
IPRL = calculated with the inelastic phonon radiation limit
PRL = calculated with the phonon radiation limit

References

[1] Cahill, D. G., Ford, W. K., Goodson, K. E., Mahan, G. D., Majumdar, A., Maris, H. J., Merlin, R., and Phillpot, S. R., 2003, "Nanoscale Thermal Transport," J. Appl. Phys., **93**, pp. 793–818.
[2] Little, W. A., 1959, "The Transport of Heat Between Dissimilar Solids at Low Temperatures," Can. J. Phys., **37**, pp. 334–349.
[3] Vincenti, W. G., and Kruger, C. H., 2002, *Introduction to Physical Gas Dynamics*, Krieger, Malabar, FL.
[4] Majumdar, A., 1993, "Microscale Heat Conduction in Dielectric Thin Films," ASME J. Heat Transfer, **115**, pp. 7–16.
[5] Swartz, E. T., and Pohl, R. O., 1987, "Thermal Resistances at Interfaces," Appl. Phys. Lett., **51**, pp. 2200–2202.
[6] Swartz, E. T., and Pohl, R. O., 1989, "Thermal Boundary Resistance," Rev. Mod. Phys., **61**, pp. 605–668.
[7] Cahill, D. G., Bullen, A., and Lee, S.-M., 2000, "Interface Thermal Conductance and the Thermal Conductivity of Multilayer Thin Films," High Temp. - High Press., **32**, pp. 135–142.
[8] Kittel, C., 1996, *Introduction to Solid State Physics*, Wiley, New York.
[9] Dames, C., and Chen, G., 2004, "Theoretical Phonon Thermal Conductivity of Si/Ge Superlattice Nanowires," J. Appl. Phys., **95**, pp. 682–693.
[10] Stevens, R. J., Zhigilei, L. V., and Norris, P. M., 2007, "Effects of Temperature and Disorder on Thermal Boundary Conductance at Solid-Solid Interfaces: Nonequilibrium Molecular Dynamics Simulations," Int. J. Heat Mass Transfer, **50**, pp. 3977–3989.
[11] Schelling, P. K., Phillpot, S. R., and Keblinski, P., 2002, "Phonon Wave-Packet Dynamics at Semiconductor Interfaces by Molecular Dynamics Simulation," Appl. Phys. Lett., **80**, pp. 2484–2486.
[12] Stevens, R. J., Smith, A. N., and Norris, P. M., 2005, "Measurement of Thermal Boundary Conductance of a Series of Metal-Dielectric Interfaces by the Transient Thermoreflectance Technique," ASME J. Heat Transfer, **127**, pp. 315–322.
[13] Costescu, R. M., Wall, M. A., and Cahill, D. G., 2003, "Thermal Conductance Of Epitaxial Interfaces," Phys. Rev. B, **67**, p. 054302.
[14] Stoner, R. J., and Maris, H. J., 1993, "Kapitza Conductance and Heat Flow Between Solids at Temperatures From 50 to 300 K," Phys. Rev. B, **48**, pp. 16373–16387.
[15] Snyder, N. S., 1970, "Heat Transport Through Helium II: Kapitza Conductance," Cryogenics, **10**, pp. 89–95.
[16] Lyeo, H.-K., and Cahill, D. G., 2006, "Thermal Conductance of Interfaces

Between Highly Dissimilar Materials," Phys. Rev. B, **73**, p. 144301.
[17] Hopkins, P. E., Stevens, R. J., and Norris, P. M., 2008, "Influence of Inelastic Scattering at Metal-Dielectric Interfaces," ASME J. Heat Transfer, **130**, p. 022401.
[18] Hopkins, P. E., and Norris, P. M., 2007, "Effects of Joint Vibrational States on Thermal Boundary Conductance," Nanoscale Microscale Thermophys. Eng., **11**, pp. 247–257.
[19] Gray, D. E., 1972, *American Institute of Physics Handbook*, McGraw-Hill, New York.
[20] Hopkins, P. E., Norris, P. M., Stevens, R. J., Beechem, T., and Graham, S., 2008, "Influence of Interfacial Mixing on Thermal Boundary Conductance Across a Chromium/Silicon Interface," ASME J. Heat Transfer, **130**, p. 062402.
[21] Huberman, M. L., and Overhauser, A. W., 1994, "Electronic Kapitza Conductance at a Diamond-Pb Interface," Phys. Rev. B, **50**, pp. 2865–2873.
[22] Chen, G., 2003, "Diffusion-Transmission Interface Condition for Electron and Phonon Transport," Appl. Phys. Lett., **82**, pp. 991–993.
[23] Chen, G., 2005, *Nanoscale Energy Transport and Conversion: A Parallel Treatment of Electrons, Molecules, Phonons, and Photons*, Oxford University Press, New York.
[24] Fugate, R. Q., and Swenson, C. A., 1969, "Specific Heat of Al_2O_3 From 2 to 25 K," J. Appl. Phys., **40**, pp. 3034–3036.
[25] Levinshtein, M. E., Rumyantsev, S. L., and Shur, M. S., 2001, *Properties of Advanced Semiconductor Materials: GaN, AlN, InN, BN, SiC, SiGe*, Wiley-Interscience, New York.